Effects of Spatial Aggregation of Initial Conditions and Forcing Data on Modeling Snowmelt Using a Land Surface Scheme

PABLO F. DORNES AND JOHN W. POMEROY

Centre for Hydrology, University of Saskatchewan, Saskatoon, Saskatchewan, Canada

ALAIN PIETRONIRO

National Hydrology Research Centre, Environment Canada, Saskatoon, Saskatchewan, Canada

DIANA L. VERSEGHY

Climate Research Division, Environment Canada, Toronto, Ontario, Canada

ABSTRACT

Small-scale topography and snow redistribution have important effects on snow-cover heterogeneity and the timing, rate, and duration of spring snowmelt in mountain tundra environments. However, land surface schemes (LSSs) are usually applied as a means to provide large-scale surface states and vertical fluxes to atmospheric models and do not normally incorporate topographic effects or horizontal fluxes in their calculations

A study was conducted in Granger Creek, an 8-km^2 catchment within Wolf Creek Research Basin in the Yukon Territory, Canada, to examine whether inclusion of the effects of wind redistribution of snow between landscape units, and slope and aspect in snowmelt calculations for tiles, could improve the simulation of snowmelt by an LSS.

Measured snow accumulation, reflecting overwinter wind redistribution of snow, was used to provide initial conditions for the melt simulation, and physically based algorithms from a small-scale hydrological model were used to calculate radiation on slopes during melt. Based on consideration of the spatial distribution of snow accumulation, topography, and shrub cover in the basin, it was divided into five landscapes units (tiles) for simulation of mass and energy balance using an LSS during melt. Effects of averaging initial conditions and forcing data on LSS model performance were contrasted against distributed simulations. Results showed that, in most of the cases, simulations using aggregated initial conditions and forcing data gave unsuccessful descriptions of snow ablation whereas the incorporation of both snow-cover redistribution and slope and aspect effects in an LSS improved the prediction of snowmelt rate, timing, and duration.

---

1. Introduction

Landscape heterogeneity has been proven to be one of the main factors that control both snow accumulation and snow-cover depletion in mountain environments (Marks et al. 2001; Pomeroy et al. 2003; Luce and Tarboton 2004). Land surface schemes (LSSs) have evolved from very simple approaches such as the

bucket model of Manabe (1969) using a conceptual representation of some of the land surface processes, to more complex approaches such as the Biosphere–Atmosphere Transfer Scheme (BATS; Dickinson et al. 1993) or the Canadian Land Surface Scheme (CLASS; Verseghy 1991; Verseghy et al. 1993) including energy and water exchanges between soil layers and explicit representations of canopy effects and snow cover.

Given that LSSs are usually applied as a means to provide the lower boundary condition to general circulation models (GCMs) or numerical weather prediction (NWPs) models, LSSs have usually focused on providing reliable large-scale surface states and vertical fluxes

Corresponding author address: Pablo Dornes, Centre for Hydrology, University of Saskatchewan, 117 Science Place, Saskatoon, SK S7N 5C8, Canada.
E-mail: pablo.dornes@usask.ca

to the atmosphere and hydrological inputs to continental-scale river forecasts. This approach has meant that small-scale horizontal processes and landscape heterogeneity were either ignored or aggregated.

Furthermore, because of the need to operate LSSs over both many and large model grids, different approaches addressed the spatially heterogeneous processes of scales smaller than the grid size. Thus, landscape heterogeneity was usually described using a grid dominant and/or composite vegetation types, whereas representation of subgrid heterogeneity varied from a statistical approaches assuming probability distributions of some landscape features or bucket sizes (e.g., Avissar and Pielke 1989; Sivapalan and Woods 1995), to more realistic representations known as mosaic approaches where the model grid is split into more than one vegetation type or tile (e.g., Koster and Suarez 1992; Verseghy et al. 1993; Essery et al. 2003). These approaches include independent calculations in each tile and allow for the inclusion of the major vegetation types and are parameterized using effective parameters assuming scale linearity between fluxes and surface characteristics (Wood 1995).

The Project for Intercomparison of Land Surface Parameterization Schemes (PILPS; Henderson-Sellers et al. 1995) had shown that different parameter set and model structures among LSS models give significantly different surfaces fluxes. In Phase 2(d) of the PILPS project the representation of the snow in LSS models was evaluated (Slater et al. 2001). PILPS 2(d) found that all LSS models were able to reproduce interannual variations of accumulation and ablation patterns, but that significant differences in the timing of the complete ablation of snow between the models were observed. Problems in representing amounts of energy incident on the portion of the grid assigned as snow, especially during ablation events at early stages of the snow season, were the cause of substantive divergences during the snow season due to internal feedback processes. Similarly, the Snow Model Intercomparison Project (SnowMIP) found a wide range of capabilities in simulating snow water equivalent (SWE) at a point during the accumulation and melt periods between the models (Etchevers et al. 2004).

Small-scale heterogeneity is especially important in arctic and subarctic mountain environments during the spring snowmelt season. Over the winter, snow is blown from areas of high wind exposure to sheltered sites, and ablates in an uneven manner (Pomeroy et al. 1997; Liston and Sturm 1998; Essery et al. 1999). This generates a highly nonuniform distribution of snow cover in the spring, which usually leads to a mosaic of snow, bare ground, and emergent vegetation as melt progresses.

Topography strongly affects the energetics and rates of snow ablation. Pomeroy et al. (2003) found that for the same basin, small differences in incoming shortwave radiation at early stages of melt between north-facing (NF) and south-facing (SF) slopes, however, significantly different half-hour average values of net radiation were observed when shrubs and bare ground emerged as the melt progresses, resulting in large positive values of net radiation to the SF, while the NF fluxes remained negative. Simulations from a blowing snow transport and sublimation model (Essery and Pomeroy 2004) showed that exposed shrubs also increased snow accumulation by suppressing snow transport and sublimation by wind due to higher aerodynamic roughness. The effects of shrub height on controlling both snow accumulation and ablation in tundra environments were also described by Liston et al. (2002) and Sturm et al. (2001). McCartney et al. (2006) found that tall shrubs play a key role in both snow accumulation and the streamflow regime; whereas Pomeroy et al. (2006) showed the importance of shrub exposure in governing snowmelt energy by enhancing melt energy due to greater longwave and sensible heat fluxes to snow.

Explicit representations of landscape heterogeneity in LSSs and land surface hydrological (LSH) models, including slope and aspect effects at small to medium basin scales in arctic and mountainous environments, have been shown to significantly improve simulations of snow-cover ablation and basin runoff compared with aggregated approaches (Déry et al. 2004; Davison et al. 2006). Effects included a more accurate description of differential snowmelt rates and an improved timing and magnitude of spring snowmelt runoff. However, fewer studies have evaluated the effects of landscape heterogeneity on melt model performance, at the landscape and basin scale, in mountain tundra environments during the snowmelt season (e.g., Dornes et al. 2008. Therefore, the objective of this study is to examine the implications of including an explicit landscape representation of snow distribution and slope and aspect in an LSS for the simulations of snow-cover ablation for a small basin in a mountain tundra environment. The evaluation is conducted by comparing the effects on model performance of aggregated to distributed initial conditions and forcing data.

2. Study basin and observations

The selected study area was Granger Basin (60°31′N, 135°07′W) which is part of Wolf Creek Research Basin
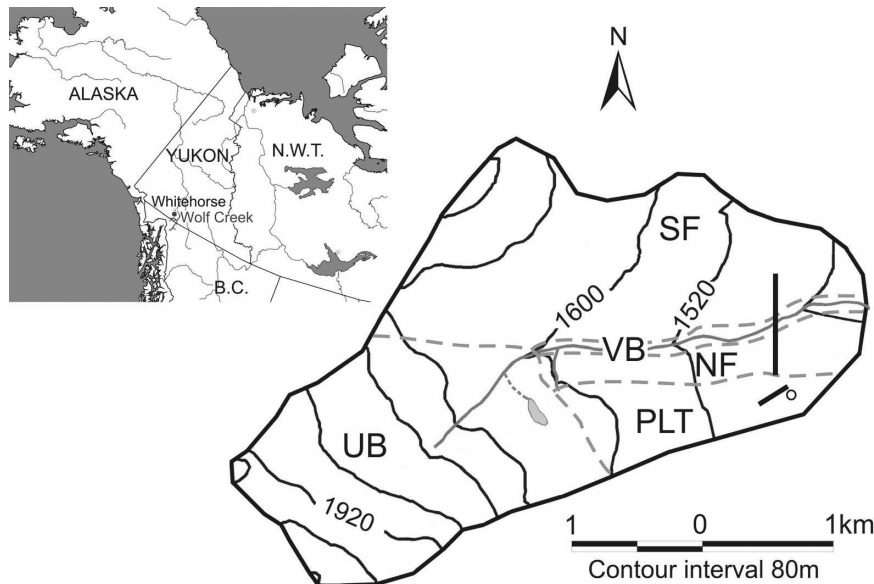
FIG. 1. Granger Basin within Wolf Creek Research Basin. Gray dashed lines demarcate landscape units: UB, PLT, NF, SF, and VB. Black solid lines show topographic contour lines. Black segments and circle indicate the location of snow survey transects and met station, respectively.

situated 15 km south of Whitehorse, Yukon Territory, Canada (Fig. 1). Granger Basin, drained by Granger Creek, is located in the mountainous headwaters of the Yukon River basin and compromises a drainage area about 8 km² ranging in elevation from 1310 to 2035 m MSL. The climate is subarctic continental characterized by a large seasonal variation in temperature ($-50°$ to $+25°C$), low precipitation (300–400 mm yr^{-1}), and low relative humidity.

The presence of permafrost varies according to aspect and temperature, thus it is found under the NF slope and in higher elevations, whereas seasonally frozen soils occur on the SF slope and the plateau (PLT) area. In the NF slope and at lower-elevation regions such as the valley bottom (VB), soils are usually capped by an organic layer up to 0.4 m thick consisting of peat, lichens, mosses, sedges, and grasses (Carey and Quinton 2005).

The landscape varies from exposed mineral soils with a sparse vegetation cover where grasses, lichens, and mosses prevail in the high-elevation areas or the upper basin (UB), to soils capped with an organic layer and a vegetation cover of tall shrubs (tall-shrub tundra) in wet, lower-elevation areas, with mineral soils covered by short shrubs (short-shrub tundra) at intermediate-elevation areas of better drainage such as the PLT area. In general, the canopy of the tall-shrub tundra consists of many isolated islands of shrubs, whereas the short-shrub tundra areas have a more homogeneous spatial structure (Bewley 2006). Table 1 summarizes the five main landscape units defined by Dornes et al. (2008), according to their exposure, vegetation cover, and soil types.

Meteorological observations of three snowmelt periods (i.e., 2002, 2003, and 2004) were used to force the models. Air temperature, relative humidity, incoming

TABLE 1. Physiographic characteristics of the landscapes units at Granger Basin. Vegetation cover and soil type were adapted from McCartney (2006) and Bewley (2006). Vegetation cover is used to parameterize the CLASS model: shrubs (S), grasses (G; also lichens, mosses, peat), and bare ground (BG; also rocks).

Landscape unit	Area (km²)	Elevation range (m)	Vegetation type	Vegetation cover (%)			Soil type
				S	G	BG	
UP	2.5	1600–2035	Bare ground	35	45	20	Mineral/rocks
PLT	1	1460–1520	Short shrubs (<0.3 m)	80	15	5	Mineral + thin organic layer (<0.1 m)
NF	1	1350–1460	Mix shrubs (0.3–1 m)	78	17	5	Thick organic layer (0.25 m) + mineral
SF	3	1350–1760	Mix shrubs (0.3–1 m)	74	20	6	Organic layer (0.12 m) + mineral
VB	0.5	1310–1350	Tall shrubs (>1 m)	71	19	10	Organic layer (0.14 m) + mineral

TABLE 2. Initial SWE in mm for each of the landscape units for the study period. The aggregated values (AGR) were calculated from the spatially weighted basin-average using the NF, SF, and VB landscape units.

	UB	PLT	NF	SF	VB	AGR
2003	187.8	138.9	218.4	275.2	172.0	251.1
2002			303.6	114.6	150.1	160.9
2004		94.8	239.6	229.9	180.8	226.6

solar and longwave radiation, wind speed and wind direction were measured on the PLT area in 2002 and 2003, whereas atmospheric pressure was measured at a nearby station at a similar elevation (1616 m MSL). For the 2004 snowmelt season, meteorological observations at the valley bottom were used. Precipitation data were obtained from a nearby station situated approximately 2 km from the study site within Wolf Creek Research Basin. No correction was performed on the precipitation data because of the insignificant amounts recorded in the studied snowmelt periods.

Snow surveys were typically conducted on a daily basis from mid-April to early June in each of the landscape units. These surveys consisted of transects where both snow depth and density were measured every 5 and 10 m, respectively. Length of the transects varied as a function of the landscape heterogeneity, thus when the snow cover was continuous a total of approximately 50 and 25 points were measured in the UB, and the PLT area, whereas 20, 20, and 6 points were measured in the NF and SF slopes, and the VB, respectively (for more details see McCartney et al. 2006). From these data, areal SWE was calculated for the UB, PLT area, NF and SF slopes, and VB landscapes. Table 2 illustrates the available snow survey transects for this study and their corresponding initial SWE values. Premelt snow accumulation showed a contrasting interannual variation among some of the landscape units. Thus, initial SWE at the SF slope was 26% larger than at the NF slope for 2003, whereas it only represented 38% of the SWE at the NF in 2002. In contrast, similar values were observed in 2004.

Canopy structure measurements such as shrub cover, vegetation height, and plant area index (PAI) were conducted along the NF, VB, SF, and PLT snow survey transects, and in a 30 m × 30 m grid (i.e., GB grid) located in the VB beside the snow survey transect (Bewley 2006). Observations of shrub cover included the use of aerial photographs from a camera mounted on a remote-controlled model helicopter, whereas PAI, defined as the ratio between the total plant surface area and the surface area of ground covered by plants was calculated using two methods, an LAI-2000 Canopy Analyzer and an upward-looking hemispherical (fish eye) camera using GLA software (Frazer et al. 1999). Values of fraction of the landscape covered by shrubs (Fs) at the VB varied from 0.20% to 0.71% at the early and late stages of the snowmelt season, respectively. Average LAI (i.e., plant area index) values were obtained using upward-looking hemispherical (fish eye) photographs taken at 5-m intervals across the GB grid and an LAI-2000 Canopy Analyzer was used along the PLT snow transect for later melt stages. Average LAI values were 0.43 for tall shrubs exposed above the snow in the VB and 0.31 in the PLT area at the end of April of 2004, whereas LAI values above 2 were measured in the summertime in different points of the basin. Values of forcings (Fs) and LAI for the remaining landscape units were estimated by comparing their canopy structure such as vegetation height and density with the measured sites and from previous LAI measurements in similar sites at Wolf Creek Research Basin.

Measurements of areal albedo (flux weighted by wavelength) above the canopy were conducted in 2003 and 2004 at the PLT area and the VB. Initial premelt albedo values for the tall and short shrubs (short shrubs were essentially an unvegetated snow field at this time) were 0.39 and 0.89, respectively. Larger and faster albedo decays were observed on the PLT area due to the abrupt change in snow-covered area as bare patches emerged when the shallow snow melted; in contrast tall shrubs areas showed a gradual albedo decay along the snowmelt season as shrubs emerged from the snow during melt of a much deeper snowpack.

3. Model descriptions

Two models, a small-scale hydrological model and a land surface scheme, were used to simulate the effects of including explicit landscape representation on the prediction of snow-cover ablation. The Cold Regions Hydrological Model (CRHM) was used to generate the distributed solar forcing for an offline version of the Canadian Land Surface Scheme (CLASS) model. Therefore, incoming solar radiation corrected by slope and aspect was precalculated using CRHM.

a. Cold Regions Hydrological Model

The CRHM is the result of extensive research in cold regions (e.g., Gray and Landine 1988; Pomeroy et al. 1998; Gray et al. 2001; Sicart et al. 2006). It has a modular structure that allows for different process representations. Thus, physically based algorithms are integrated in the model through different modules such as radiation, infiltration into frozen soils, snow intercep-
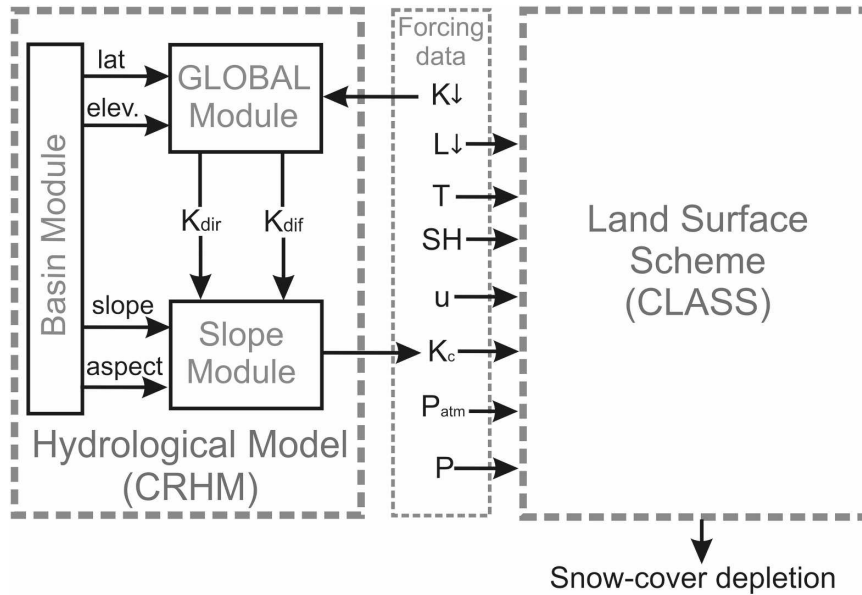
FIG. 2. Outline of the coupled modeling strategy applied: CRHM and CLASS (version 3.3). Solid arrows indicate module and model input/outputs. Here K is incoming shortwave radiation (W m^{-2}), L is incoming longwave radiation (W m^{-2}), T is air temperature (°C), SH is specific humidity (g g^{-1}), u is wind speed (m s^{-1}), K_c is corrected incoming shortwave radiation (W m^{-2}), P_{atm} is atmospheric pressure (hPa), P is precipitation flux (kg m^2 s^{-1}), K_{dir} is direct shortwave radiation (W m^{-2}), and K_{dif} is diffuse shortwave radiation (W m^{-2}).

tion, snow transport, snowmelt, etc., that finally route the water via different pathways. The spatial representation is based on the Hydrological Response Unit (HRU) concept. For details in the generic model framework see Pomeroy et al. (2007) and for details in a related application see Dornes et al. (2008).

In this study, HRUs were defined according to landscapes units. Three modules were used (Fig. 2). In the BASIN module, all the basin specifications such as HRU elevation, slope and aspect, soil type, and vegetation-cover characteristics were set.

The partitioning of the incoming solar radiation into direct beam and diffusive components for clear skies is accomplished within the GLOBAL module using theoretical formulations based on those proposed by Garnier and Ohmura (1970). Thus, the theoretical clear-sky solar radiation (K_{theo}) over flat areas is computed as the sum of the direct and diffuse incoming shortwave radiation. The cloudiness index (c) is calculated from the relation between the observed incoming shortwave radiation (K_{obs}) and the estimated K_{theo} on the horizontal surface.

Corrections for slope and aspect and cloudiness conditions are calculated in the SLOPE module. The same cloudiness index for the slope is assumed. It is then used to calculate the incoming shortwave radiation (K_c) to slopes having some aspect as, $K_c = c \, (K_{dir} + K_{dif})$,

where K_{dir} and K_{dif} are the direct and diffusive portions, respectively, of the solar radiation, as affected by slope and aspect.

b. Canadian Land Surface Scheme

The CLASS, introduced by Verseghy (1991) and Verseghy et al. (1993), has been widely used in Canada as the LSS for the Canadian GCM and also coupled to a hydrological routing model, which was known as the WATCLASS model (Soulis et al. 2000). In this study, CLASS version 3.3 is used.

CLASS includes a physically based treatment of energy and moisture fluxes between the vegetation canopy, the snow cover, and the soil layers. The snow model uses a coupled energy and mass balance at the top and bottom of the snowpack to calculate an internal energy state. When the surface temperature or the average layer temperature rises above 0°C, this excess energy is used to melt part of the snowpack and the temperature is set back to 0°C. Snow albedo and density vary with time according to exponential functions. Snow cover is assumed to be complete above a limiting depth of 0.10 m (D100); otherwise fractional snow coverage is calculated through the employment of a snow-cover depletion curve (Donald et al. 1995). Meltwater from the surface percolates through the snowpack and
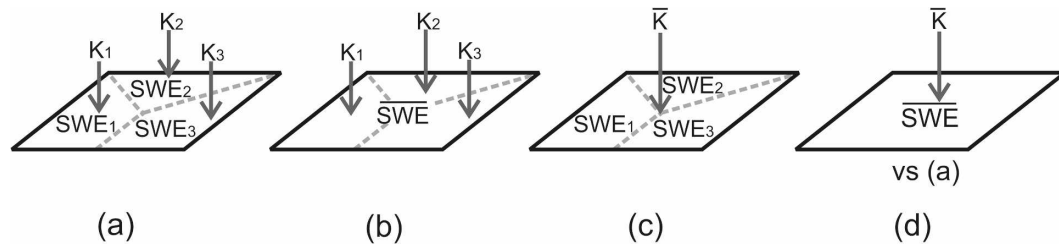
FIG. 3. Schematic illustration of the modeling approaches used to simulate snow-cover ablation showing the basin and three hypothetical landscape units. (a) Distributed initial conditions (SWE) and forcing data (K), (b) basin-average initial SWE and distributed K, (c) distributed SWE and basin-average K, (d) comparison between aggregated (basin-average SWE and K) and distributed [reaggregated values of (a)] modeling approaches.

refreezes until the temperature of the snowpack reaches the melting point. After the snowpack water-holding capacity of 0.04 kg kg^{-1} has been filled any further melt reaches the base of the snowpack.

Vegetation canopies in CLASS can be represented by four main vegetation types: needleleaf, broadleaf, crops, and grass. Each vegetation type is treated separately, and composite canopy values (e.g., albedo, roughness length, standing mass) are obtained by averaging them. Distributed versions of CLASS such as the Modélisation Environnementale Communautaire (MEC)–Surface and Hydrology (MESH) model (Pietroniro et al. 2007) make use of the Group Response Unit (GRU) concept (Kouwen et al. 1993) to handle spatial heterogeneity. Thus, predefined model grids are subdivided into tiles according to land-cover classes; which can be located anywhere in the model domain. Each tile or landscape unit has the same parameterization with four subareas: snow, bare ground, canopy over snow, and canopy over bare ground. Additionally a nonvegetation-cover type, rock or urban, is included in the calculations. For more details see Pohl et al. (2005).

4. Model configurations

a. Spatial representation

The spatial model structure was selected based on an understanding of the snow accumulation and melt characteristics of the basin derived from several years of field investigation and hydrological modeling. Delineation of mass balance calculations into landscape units having specific locations in the basin has been demonstrated to be essential not only during winter snow accumulation and posterior snow redistribution by wind (Pomeroy et al. 1997; Essery and Pomeroy 2004), but also, in the contrasting runoff production among the different landscape units due to differential snowmelt rates as a result of vegetation characteristics (Liston 1999; McCartney 2006; Pomeroy et al. 2006). Slope and aspect (Pomeroy et al. 2003), advection from bare ground (Marsh and Pomeroy 1996; Essery et al. 2006; Granger et al. 2006), and of infiltration and soil towing (Carey and Quinton 2005; Quinton et al. 2005), also showed identifiable landscape characteristics. These findings mean that the incorporation of spatially ex-

TABLE 3. Optimized parameter values for the different landscape units (Stomatal = STL, stomata = STO, snow cover = SC). Parentheses indicate parameter bounds.

Parameter	UB		PLT	
	Shrub	Grass	Shrub	Grass
Max LAI (LAMX)	1.5 (1, 1.5)	1.9 (0.5, 2)	2.17 (2, 2.5)	0.53 (0.5, 2)
Min LAI (LAMN)	0.50 (0.4, 0.5)	0.31 (0.1, 0.4)	0.50 (0.4, 0.5)	0.28 (0.5, 3)
LN roughness length (LNZ0) (m)	−3.65 (−3.7, −3.2)	−3.69 (−5.3, −3.7)	−3.66 (−3.7, −2.3)	−4.09 (−4.8, −3.5)
Visible albedo (ALVC)	0.031 (0.03, 0.2)	0.081 (0.02, 0.2)	0.032 (0.03, 0.2)	0.183 (0.02, 0.2)
Near-infrared albedo (ALIC)	0.303 (0.3, 0.5)	0.310 (0.2, 0.5)	0.302 (0.3, 0.5)	0.424 (0.2, 0.4)
Biomass density (CMAS) (kg m^{-2})	1.74 (1, 5)	0.08 (0.05, 0.35)	3.06 (3, 7)	0.11 (0.05, .35)
Min STL resistance (RSMN)	175.0 (50, 300)	91.6 (50, 300)	145.1 (50, 300)	251.5 (50, 300)
Coef STO response to light (QA50) (W m^{-2})	40.6 (20, 60)	27.3 (20, 60)	58.3 (20, 60)	46.1 (20, 60)
Coef STL resistance to VP deficit (VPDA)	1.13 (0.2, 1.5)	1.47 (0.2, 1.5)	1.19 (0.2, 1.5)	1.31 (0.2, 1.5)
Coef STL resistance to VP deficit (VPDB)	0.61 (0.2, 1.5)	0.70 (0.2, 1.5)	0.61 (0.2, 1.5)	0.61 (0.2, 1.5)
Coef STL resistance to soil WS (PSGA)	96.8 (50, 150)	130.0 (50, 150)	81.6 (50, 150)	146.7 (50, 150)
Coef STL resistance to soil WS (PSGB)	2.08 (1–10)	6.01 (1, 10)	2.57 (1–10)	4.92 (1, 10)
Min avg depth 100% SC (D100) (m)	0.90 (0.01, 1)		0.42 (0.01, 0.5)	

plicit landscape units in LSSs may improve both model predictions and feedbacks to atmospheric models. Therefore, the basin was divided into five distinct zones that represent different landscape units that were set as GRU. Independent LSS runs were conducted for each landscape unit.

b. Modeling strategy

To account for slope and aspect effects, first, corrected incoming solar radiation was calculated using CRHM in the UB, and NF and SF slopes, whereas observations of solar radiation without correction were applied in the horizontal landscape units such as the PLT and VB. These data along with the complementary meteorological observations were used as forcing data for CLASS (see Fig. 2). Thus, snow-cover ablation was evaluated using CLASS in a point or one-dimensional mode (i.e., as a vertical column) for each landscape unit.

Four modeling approaches were tested and compared (Fig. 3): 1) distributed simulations of SWE using both distributed initial conditions and forcing data; 2) distributed simulations of SWE using aggregated (i.e., basin average) initial conditions but distributed forcing data; 3) distributed simulations of SWE using distributed initial conditions but aggregated forcing data; and 4) comparison of simulations of SWE using aggregated (i.e., initial conditions and forcing data) and distributed (i.e., reaggregated values of point 1) modeling approaches.

c. Model parameterization and initial conditions

To test the different modeling strategies, CLASS was automatically calibrated in 2003 and the results were validated in 2002 and 2004, respectively. The selection of 2003 as the calibration period was based on data availability since 2003 was the year with snow surveys in each of the landscape units (see Table 2).

Effective parameter sets for each landscape unit were found using the Dynamically Dimensioned Search (DDS) global optimization algorithm (Tolson and Shoemaker 2007) and were used as model parameterizations for testing the effects of aggregating both initial conditions and forcing data. The calibration was performed over 25 parameters that control snowmelt in CLASS (Table 3). Parameters of the two dominant vegetations types, shrub and grass (see Table 1), were allowed to vary, whereas parameters for bare ground or rock were maintained constant. The calibration problem was formulated using as a single objective function, the root-mean-square error (RMSE) with respect to the SWE observations during melt. Independent calibration was performed in each of the landscape units, and optimum parameter sets were obtained after performing 500 model simulations using the DDS algorithm. The selection of the number of simulations was based on the algorithm efficiency. After 100 model simulations DDS was generally able to find good and steady solutions. Since the simulation time was not a limitation (~20 s), the number of simulations was increased to 500 to ensure that a global minimum with respect to the objective function in the parameter space was found.

Parameter ranges were restricted according to both distributed observations at Granger Basin (e.g., McCartney 2006; Bewley et al. 2007) and prior information (e.g., Verseghy et al. 1993; Kite and Spence 1994; Davison et al. 2006) for northern and mountainous environments. Table 3 shows the optimized parameter values and their corresponding ranges for the two dominant

TABLE 3. *(Extended)*

NF		SF		VB	
Shrub	Grass	Shrub	Grass	Shrub	Grass
2.81 (2, 3)	1.95 (0.5, 2.5)	2.73 (2, 3)	2.0 (0.5, 2.5)	2.98 (2.5, 3)	0.64 (0.5, 3)
0.99 (0.4, 1)	0.29 (0.5, 3)	0.60 (0.4, 1)	0.24 (0.5, 3)	0.80 (0.4, 1)	0.29 (0.5, 3)
−2.42 (−3.7, −1.8)	−3.72 (−4.8, −3.5)	−1.87 (−3.7, −1.8)	−3.12 (−4.8, 3.5)	−1.89 (−1.9, −1.3)	−3.08 (−4.8, −3.5)
0.087 (0.03, 0.2)	0.178 (0.02, 0.2)	0.033 (0.03, 0.2)	0.199 (0.02, 0.2)	0.030 (0.03, 0.2)	0.025 (0.02, 0.2)
0.464 (0.3, 0.5)	0.446 (0.2, 0.5)	0.326 (0.3, 0.5)	0.448 (0.2, 0.5)	0.301 (0.3, 0.5)	0.250 (0.2, 0.5)
6.13 (6, 10)	0.19 (0.05, 0.35)	7.08 (6, 10)	0.07 (0.05, .35)	8.53 (7, 11)	0.19 (0.05, 0.35)
51.9 (50, 300)	140.5 (50, 300)	115.8 (50, 300)	214.9 (50, 300)	104.9 (50, 300)	268.4 (50, 300)
21.1 (20, 60)	37.6 (20, 60)	38.4 (20, 60)	35.3 (20, 60)	47.2 (20, 60)	49.9 (20, 60)
1.08 (0.2, 1.5)	0.87 (0.2, 1.5)	1.28 (0.2, 1.5)	0.63 (0.2, 1.5)	0.32 (0.2, 1.5)	1.42 (0.2, 1.5)
0.93 (0.2, 1.5)	0.23 (0.2, 1.5)	0.78 (0.2, 1.5)	0.89 (0.2, 1.5)	1.21 (0.2, 1.5)	0.46 (0.2, 1.5)
93.5 (50, 150)	135.6 (50, 150)	87.7 (50, 150)	141.1 (50, 150)	71.8 (50, 150)	76.3 (50, 150)
1.09 (1–10)	1.15 (1, 10)	1.23 (1–10)	5.09 (1, 10)	4.30 (1, 10)	2.18 (1, 10)
0.81 (0.01, 1)		0.86 (0.01, 1)		0.44 (0.01, 0.5)	
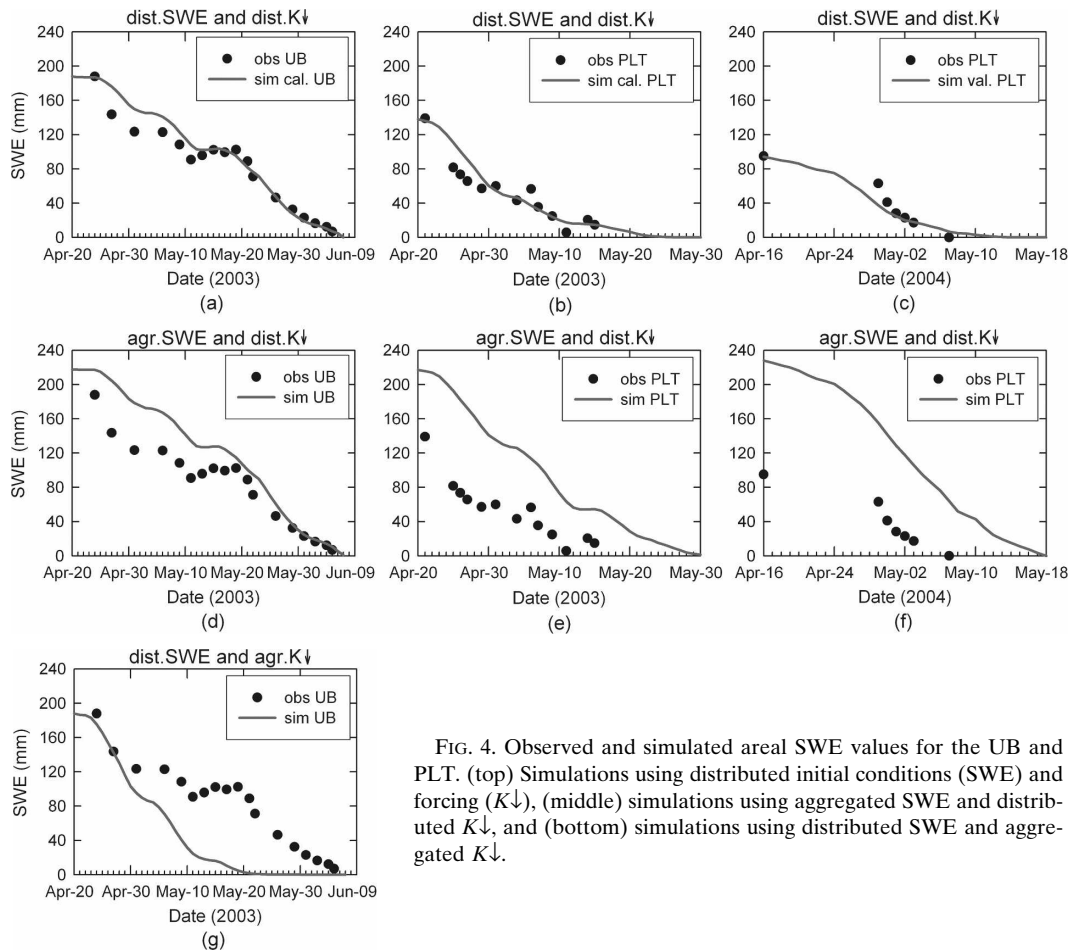
FIG. 4. Observed and simulated areal SWE values for the UB and PLT. (top) Simulations using distributed initial conditions (SWE) and forcing ($K\downarrow$), (middle) simulations using aggregated SWE and distributed $K\downarrow$, and (bottom) simulations using distributed SWE and aggregated $K\downarrow$.

land covers (i.e., shrubs and grass) in each landscape unit. Although optimum parameter sets varied among the landscape units, these variations showed consistent values with respect to the observations.

Initial conditions such as snow density and snow mass needed for CLASS were extracted from snow survey observations. Soil temperatures were obtained from observations in all the landscape units using buried thermocouples. Temperatures of the canopy were set to match the air temperature. As for premelt conditions, no ponded water was considered and minimal liquid water content was assumed for the entire soil column.

5. Results and discussion

Simulations results (Figs. 4–7) are grouped according to both landscape units, except for the Fig. 4, which combines results of the UB and the PLT area with fewer years of observations, and modeling approach. Thus, the first row in the figures illustrates the simulations using distributed initial conditions and forcing

data, the second row shows the simulations using aggregated initial conditions and distributed forcing data, and the last row displays the simulations using distributed initial conditions and aggregated forcing data (see Table 3 for available observations).

a. Simulations using distributed initial conditions and forcing data

Distributed simulations of SWE and available observations for the calibration period in 2003 are shown in Figs. 4a–7a for the UB, PLT, NF and SF slopes, and VB respectively. Simulations represent the model performance of the optimum parameter set for each landscape unit obtained from the DDS algorithm. An accurate simulation of the snow cover ablation during the melt period was observed for all the landscape units analyzed showing that CLASS could be successfully optimized to describe the different snowmelt rates, timing, and duration of the melt observed among the landscape units. Thus, higher Nash Sutcliffe (NS) coefficient values (Table 4) were seen in contrasting conditions from
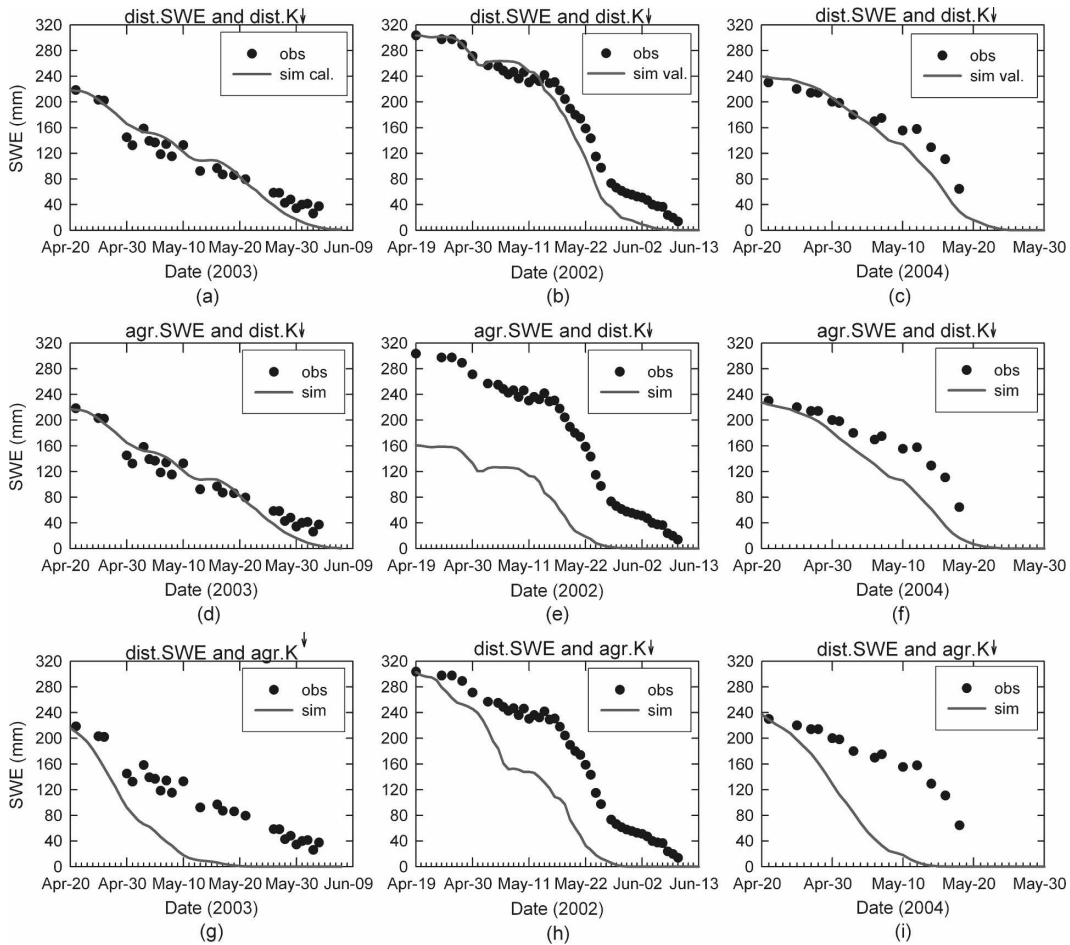
FIG. 5. Observed and simulated areal SWE values for the NF slope. (top) Simulations using distributed initial conditions (SWE) and forcing ($K\downarrow$), (middle) simulations using aggregated SWE and distributed $K\downarrow$, and (bottom) simulations using distributed SWE and aggregated $K\downarrow$.

slow and uniform snowmelt rates such as on the UB and NF (Figs. 4a and 5a) with NS values of 0.93 and 0.87, respectively, to more variable melt rates on the PLT area (Fig. 4b) with a NS value of 0.76 and in an area covered by tall shrubs as the VB (Fig. 7a) with a NS value of 0.98. However, an unsatisfactory performance was observed for the SF slope. While the rapid ablation at early stages of the snowmelt period was adequately simulated, the observed low melt rates at late stages were not seen as well (Fig. 6a).

Figures 4c; 5b,c; 6b,c; and 7b,c display the validated SWE simulations for the different landscape units, using the parameter set calibrated in 2003, for 2002 and 2004 when data was available (see Table 3). In general, similar results than in the calibration period were observed for all the landscape units analyzed. Higher performance criteria with NS values of 0.86, 0.89, and 0.94 that matched both the timing and duration of the melt were seen in the PLT in 2004 (Fig. 4c), in the SF slope

in 2002 (Fig. 6b), and in the VB in 2004 (Fig. 7c), respectively. A substantially better model performance than in the calibration period was seen in the SF in 2002 as a result of the spatial covariance between a low initial SWE and a large melt energy. Despite the faster melt rate simulated in the late stages of the melt in the NF slope (Figs. 5b,c) for 2002 and 2004, in the SF slope for 2004 (Fig. 6c), and in the VB for 2002 (Fig. 7b); reasonable performance criteria with NS values of 0.92, 0.72, 0.73, and 0.78, respectively, were seen.

b. Simulations using aggregated initial conditions and distributed forcing data

Distributed simulations of SWE using a basin-aggregated (i.e., homogeneous) initial snow cover but distributed forcing data are shown in Figs. 4d–f, 5d–f, 6d–f, and 7d–f for the calibration and validation seasons, respectively. These simulations represent the model performance in each landscape unit of the opti-
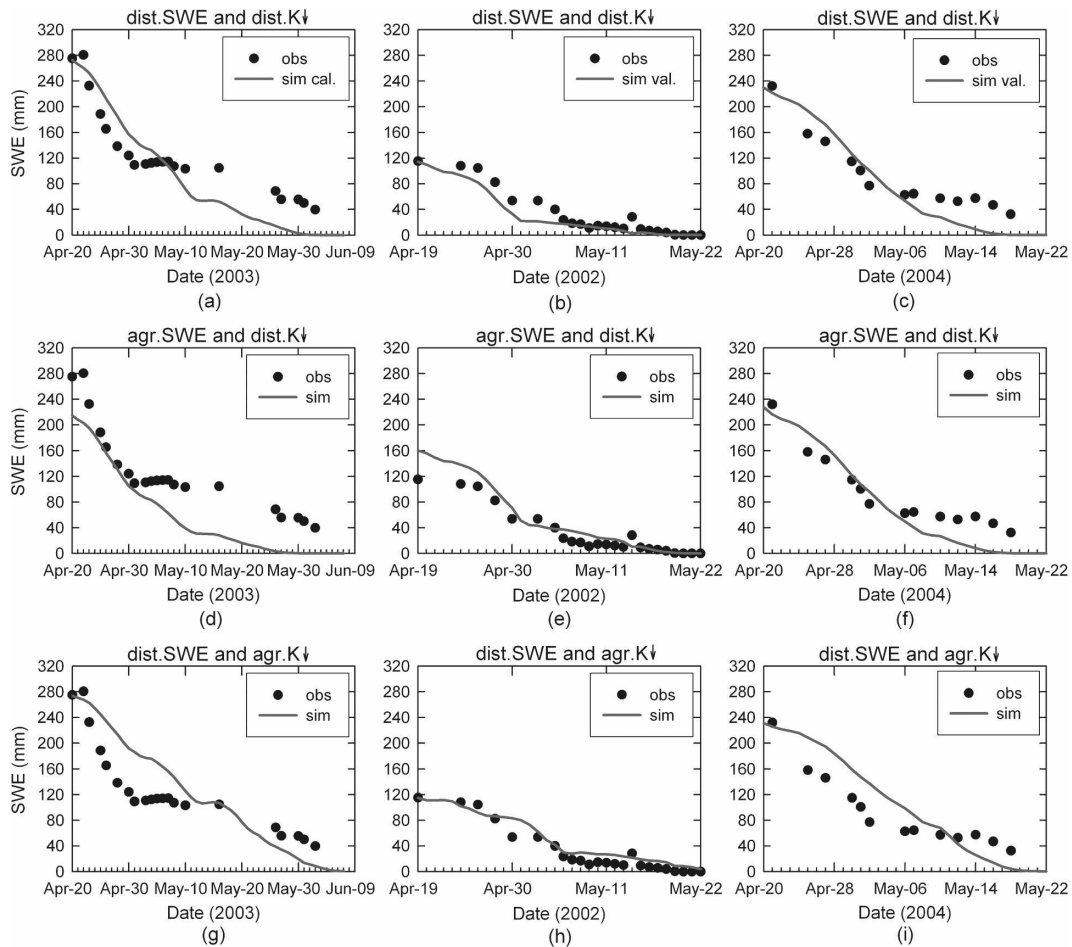
FIG. 6. Observed and simulated areal SWE values for the SF slope. (top) Simulations using distributed initial conditions (SWE) and forcing ($K\downarrow$), (middle) simulations using aggregated SWE and distributed $K\downarrow$, and (bottom) simulations using distributed SWE and aggregated $K\downarrow$.

mum parameter set calibrated in 2003, when no redistribution of the winter snow is considered.

Obvious discrepancies with the observed values were seen mainly at early stages of the snowmelt season in those landscape units where the aggregated initial SWE value did not agree with the observed value (Figs. 4e,f and 5e). Therefore, negative NS values (see Table 4) indicating unacceptable model performance, were found at the PLT area and the NF slope. For those landscape units where the initial differences were not substantial, differences between simulated and observed values, resulted in similar snowmelt rates along the snowmelt season; however, model performance was degraded in almost all the cases.

c. Simulations using distributed initial conditions and aggregated forcing data

The effects of using homogeneous forcing data (incoming shortwave) without considering slope and as-

pect effects but using distributed aggregated conditions on simulating distributed SWE values are shown in Figs. 4–6 for the UB, NF, and SF slopes, respectively. Lower performance criteria compared with those runs using distributed forcing were found in all the landscapes studied (Table 4). Simulations showed markedly higher melt rates as compared to the observed values that resulted in a significant shortening of the snowmelt season. This is illustrated by negative NS values in the UB in 2003 (Fig. 4g) and by negative or very low NS values in NF slope (Figs. 5g–i). On the other hand, these effects were less noticeable on the SF slope presumably because of the weakness on simulating snowmelt of the model parameterization obtained using distributed forcing in 2003. Simulations showed more uniform melt rates than both the simulations using distributed forcings and the observations. As a result the duration of the snowmelt seasons were lengthened and model performances were degraded when more
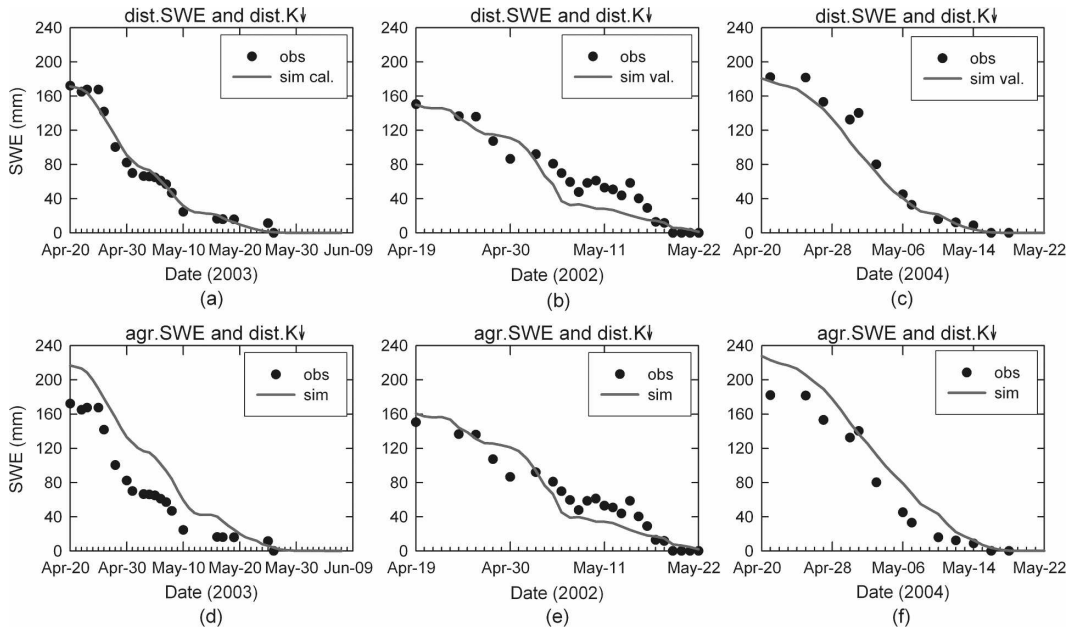
FIG. 7. Observed and simulated areal SWE values for the VB. (top) Simulations using distributed initial conditions (SWE) and forcing ($K\downarrow$) and (bottom) simulations using aggregated SWE and distributed $K\downarrow$.

accumulation was observed such in 2003 and 2004 (Figs. 6g,i). In the 2002 snowmelt season (Fig. 6h), although a high model performances was observed (NS = 0.87), the estimation of the duration of the snowmelt season was lengthened by approximately 6 days.

d. Aggregated versus distributed modeling approaches

Figure 8 illustrates the comparison of the simulated basin-scale snow-cover ablation using both an aggregated and distributed modeling approaches. The aggregated model used the basin average of both SWE and incoming solar radiation (see Fig. 3d), whereas in order to compare both modeling approaches, the distributed model used the reaggregated distributed model outputs from each landscape unit. Comparisons were performed on those landscape units where snow survey data were available in all of the 3 yr compared; hence, observations were spatially weight averaged. Thus, only the NF and SF slopes, and VB were considered. The model parameterization was also set by using the spatial weight average of the optimum parameter sets obtained in 2003 in the three landscapes considered.

TABLE 4. Comparison of model performance in each landscape unit: Initial condition (IC), forcing (F), RMSE, Nash–Sutcliffe coefficient (NS). Performances for the calibration period are shown in bold.

Modeling strategy	Yr	UB		PLT		NF		SF		VB	
		RMSE (mm)	NS	RMSE (mm)	NS	RMSE (mm)	NS	RMSE (mm)	NS	RMSE (mm)	NS
Distributed IC and F	2003	**13.3**	**0.93**	**16.7**	**0.76**	**19.6**	**0.87**	**36.2**	**0.70**	**8.8**	**0.98**
	2002					28.0	0.92	12.0	0.89	19.4	0.78
	2004			10.8	0.86	25.5	0.72	28.3	0.73	16.3	0.94
Aggregated IC	2003	31.4	0.58	81.8	−4.87	19.5	0.87	44.9	0.54	41.6	0.46
	2002					112.3	−0.36	17.9	0.75	17.0	0.83
	2004			100.3	−10.69	44.2	0.16	27.7	0.74	27.0	0.84
Aggregated F	2003	**57.1**	**−0.38**			**65.9**	**−0.44**	**44.9**	**0.54**		
	2002					78.4	0.34	12.8	0.87		
	2004					101.3	−3.44	37.3	0.54		
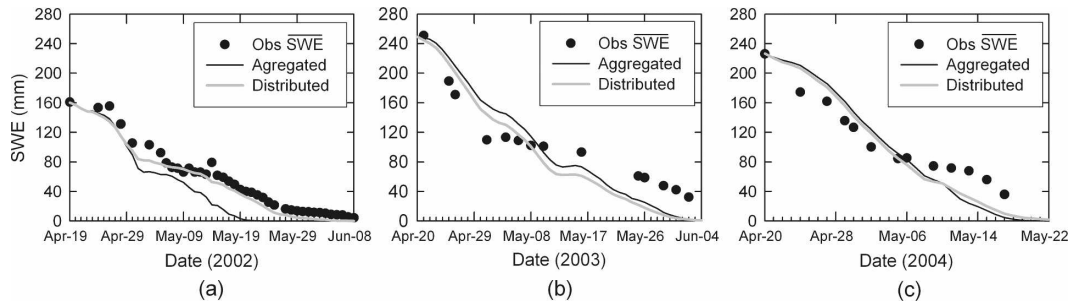
FIG. 8. Comparison between spatially weighted basin-average simulations of SWE using aggregated (i.e., initial conditions and forcing data) and distributed (reaggregated) modeling approaches: (a) 2002, (b) 2003, and (c) 2004.

Dissimilar model performances were observed for the considered years. Differences between aggregated and distributed modeling approaches were small in 2003 and 2004 (Figs. 8b,c) due to the reduction in the spatial variability of the initial SWE compared to 2002 (Fig. 8a). For the 2002 snowmelt season, simulated SWE values of both the aggregated and the distributed models showed a close agreement with the observations at the early stages of the snowmelt season; however, model results diverged in late melt. The distributed model adequately described the snow-cover ablation with a NS value of 0.96 (Table 5), whereas the aggregated model was unable to simulate the later half of the melt, showing a much more rapid depletion than the observed with a NS decreasing to a value of 0.68. This difference in performance resulted in an increase of the RMSE from 9 to 24.5 mm of SWE. Conversely, for the 2003 and 2004 snowmelt periods, simulated SWE values of both the aggregated and the distributed models exhibited a very similar description of the evolution of the snow-cover depletion. Analysis of the model performances showed NS values for the aggregated and distributed model of 0.70 and 0.72 for 2003 and 0.74 and 0.80 for 2004, respectively. Similar performances in terms of the RMSE were also observed.

One of the possible reasons that may explain the dissimilar results from the comparisons between the aggregated and the distributed approaches could be related to the differences in the ratio of the initial SWE on the NF and SF slopes among the analyzed snowmelt seasons. The 2002 snowmelt season showed a very high spatial variability of the initial SWE with 303 and 120 mm of SWE in the NF and SF slopes, respectively, resulting in a difference of 39%. Conversely in 2003 the SF slope showed higher initial SWE values (280 mm) than those seen in the NF slope (230 mm) resulting in a difference of 26% whereas similar initial SWE values were observed in 2004. As a result larger differences between the aggregated and distributed approaches were seen when the differences in the initial SWE increased. Another reason could be the spatial covariance between initial SWE and melt energy. The coincidence of low SWE and high melt energy on the SF slope in 2002 raised the spatial variability of the snow cover depletion (SCD), whereas the coincidence of high SWE and high melt rate (i.e., 2003 and 2004) reduced the variability of the SCD. Additionally, the high-subgrid variability of SWE due to the presence of an unusual drift in the SF slope (McCartney 2006) not properly considered in the spatial discretization of the model may explain why unsatisfactory simulations were observed on the SF slope for 2003 and 2004. Therefore, and given the areal dominance of the SF, no significant differences were observed between the aggregated and the distributed modeling approaches.

6. Conclusions

The enhancement of LSS simulations of snow-cover depletion by including an explicit representation of the landscape heterogeneity was analyzed. The study included the comparison of model performance between a distributed and a basin-aggregated modeling approaches in a subarctic mountainous environment. The effects of aggregating initial conditions and forcing data such as incoming solar radiation were also evaluated.

TABLE 5. Comparison of model performance between the basin-aggregated (AGR) and distributed (DIST) modeling approach. RMSE and NS (defined in Table 4) are shown. Performances for the calibration period are shown in bold.

	AGR		DIST	
Yr	RMSE (mm)	NS	RMSE (mm)	NS
2003	**32.2**	**0.70**	**28.8**	**0.72**
2002	24.5	0.68	9.0	0.96
2004	26.7	0.74	23.1	0.80

The modeling strategy has been formulated applying a combined approach. First, the landscape heterogeneity is explicitly represented in the model (i.e., basin division) based on the previous understanding of the main controls over the hydrological processes in this environment. On this basis, a detailed description was used to generate the physically based forcing data and process representations. This was also achieved in the context of a calibration problem, where the effective parameters values were automatically optimized to best represent the complexity of the system.

Results showed that CLASS, using the preprocessing of the incoming shortwave radiation by CRHM, was able to successfully describe the snow-cover ablation in the landscape units studied. Tiled simulations in the different landscapes using distributed information accurately described the observed snowmelt rates and timing of the melt. This highlights the importance of including spatially distributed information such as snow redistribution and topography in order to reduce input uncertainty.

Conversely, the conceptualization of the model grid as a single flat unit was not always able to properly describe the observed snow ablation. Simulations using such an aggregated approach when the spatial variability of the SWE increased or when the covariance between SWE and energy inputs was negative, showed a degradation of model performance, compared to the distributed model. This was illustrated in 2002 with the greatest discrepancies between the two approaches resulting in a reduction of the NS coefficient from 0.96 to 0.68. However, in those years when less spatial variability of the SWE was observed as a result of more homogeneous redistribution of snow with a positive covariance between accumulation and melt, there were no substantial differences between the aggregated and distributed modeling approaches. On the contrary, the distributed approach adequately described the snow-cover ablation in all the cases.

The effect of aggregating the initial conditions by using a basin-average initial snow-cover (i.e., no snow redistribution) degraded model performance. In most cases examined, the differences with the observed initial SWE in each landscape unit were drastic, resulting in unsuitable model predictions. The effects were more noticeable in those landscapes units with high wind exposure (e.g., PLT) and sheltered sites (e.g., NF slope) with respect to the predominant winds. These results emphasize the importance for hydrological model predictions of incorporating snow-cover heterogeneity caused by wind redistribution to reduce uncertainty in process descriptions.

Aggregation of forcing data (i.e., radiation not corrected for slope and aspect effects) also had unfavorable effects on model predictions. Thus, the assumption of uniform topography within the model grid significantly shortened or lengthened the duration of the melt in the NF and SF slopes, respectively, which resulted in inappropriate model predictions represented by negative NS values and unreasonable larger RMSE values. However, it should be stressed that despite the effects due to either initial conditions or forcing data, the combined effects as a result of the positive covariance between accumulation and melt are smaller and sometimes unimportant.

In summary, the consideration of snow-cover heterogeneity due to wind redistribution and the effects of small-scale topography on melt energetics enhanced predictions of snow ablation. This is also consistent with the findings in Déry et al. 2004, Davison et al. 2006, and Dornes et al. (2008) in arctic and subarctic environments, where distributed approaches led to enhanced model simulations of LSS and hydrological models. Therefore, the incorporation of explicit representation of the landscape heterogeneity in LSSs can improve the estimate of snow-covered area, melt rate, and land surface–atmospheric interaction at both small and larger scales.

REFERENCES

Avissar, R., and R. Pielke, 1989: A parameterization of heterogeneous land surfaces for atmospheric numerical models and its impact on regional meteorology. *Mon. Wea. Rev.,* **117,** 2113–2136.

Bewley, D., 2006: Shrub-tundra effects on snowmelt energectics and the atmospheric interaction with snow. Ph.D. thesis, University of Wales, Aberystwyth, Wales, 211 pp.

——, J. W. Pomeroy, and R. L. H. Essery, 2007: Solar radiation transfer through a sub-arctic shrub canopy. *Arct. Alp. Res.,* **39,** 365–374.

Carey, S. K., and W. L. Quinton, 2005: Evaluation of runoff generation during summer using hydrometric, stable isotope and hydrochemical methods in a discontinuous permafrost environment. *Hydrol. Processes,* **19,** 95–114.

Davison, B., S. Pohl, P. Dornes, P. Marsh, A. Pietroniro, and M. MacKay, 2006: Characterizing snowmelt variability in a land surface hydrologic model. *Atmos.–Ocean,* **44,** 271–287.

Déry, S. J., W. T. Crow, M. Stieglitz, and E. F. Wood, 2004: Modeling snow-cover heterogeneity over complex arctic terrain for regional and global climate models. *J. Hydrometeor.,* **5,** 33–48.

Dickinson, R. E., A. Henderson-Sellers, and P. J. Kennedy, 1993: Biosphere Atmosphere Transfer Scheme (BATS) version 1e as coupled to the NCAR Community Climate Model. NCAR/NT-387+STR, National Center for Atmospheric Research, Boulder, CO, 72 pp.

Donald, J. R., E. D. Soulis, N. Kouwen, and A. Pietroniro, 1995: Snowcover depletion curves and satellite snowcover estimates for snowmelt runoff modelling. *Water Resour. Res.,* **31,** 995–1009.

Dornes, P. F., J. W. Pomeroy, A. Pietroniro, S. K. Carey, and W. L. Quinton, 2008: Influence of landscape aggregation in modelling snow-cover ablation and snowmelt runoff in a subarctic mountainous environment. *Hydrol. Sci. J.,* in press.

Essery, R. L. H., and J. W. Pomeroy, 2004: Vegetation and topographic control of wind-blown snow distributions in distributed and aggregated simulations for an arctic tundra basin. *J. Hydrometeor.,* **5,** 734–744.

——, L. Li, and J. W. Pomeroy, 1999: A distributed model of blowing snow fluxes over complex terrain. *Hydrol. Processes,* **13,** 2423–2438.

——, M. J. Best, R. A. Betts, P. M. Cox, and C. M. Taylor, 2003: Explicit representation of subgrid heterogeneity in a GCM land surface scheme. *J. Hydrometeor.,* **4,** 530–543.

——, R. Granger, and J. Pomeroy, 2006: Boundary-layer growth and advection of heat over snow and soil patches: Modelling and parameterization. *Hydrol. Processes,* **20,** 953–967.

Etchevers, P., and Coauthors, 2004: Validation of the surface energy budget simulated by several snow models (SnowMIP project). *Ann. Glaciol.,* **38,** 150–158.

Frazer, G. W., C. D. Canham, and K. P. Lertzman, 1999: Gap light analyser GLA, version 2.0: Imaging software to extract canopy structure and gap light transmission indices from true-color fisheye photographs. User manual and program documentation, Simon Fraser University and Institute of Ecosystem Studies, 40 pp.

Garnier, B. J., and A. Ohmura, 1970: The evaluation of surface variations in solar radiation income. *Sol. Energy,* **13,** 21–34.

Granger, R. J., R. Essery, and J. W. Pomeroy, 2006: Boundary-layer growth over snow and soil patches: Field observations. *Hydrol. Processes,* **20,** 943–951.

Gray, D. M., and P. G. Landine, 1988: An energy-budget snowmelt model for the Canadian Prairies. *Can. J. Earth Sci.,* **25,** 1292–1303.

——, B. Toth, L. Zhao, J. W. Pomeroy, and R. J. Granger, 2001: Estimation areal snowmelt infiltration into frozen soils. *Hydrol. Processes,* **15,** 3095–3111.

Henderson-Sellers, A., A. J. Pitman, P. K. Love, P. Irannejad, and T. H. Chen, 1995: The Project for Intercomparison of Land Surface Parameterization Schemes (PILPS): Phases 2 and 3. *Bull. Amer. Meteor. Soc.,* **76,** 489–503.

Kite, G. W., and C. Spence, 1994: Land cover, NDVI, LAI and evapotranpsiration in hydrological modelling. *Application of Remote Sensing in Hydrology, Proceedings of the Second International Workshop, Meteor. Monogr.,* No. 14, NHRI, 223–239.

Koster, R., and M. J. Suarez, 1992: Modeling the land surface boundary in climate models as a composite of independent vegetation stands. *J. Geophys. Res.,* **97,** 2697–2715.

Kouwen, N., E. D. Soulis, A. Pietroniro, J. Donald, and R. A. Harrington, 1993: Grouped response units for distributed hydrological modeling. *J. Water Resour. Plann. Manage.,* **119,** 289–305.

Liston, G. E., 1999: Interrelationships among snow distribution, snowmelt, and snow cover depletion: Implications for atmospheric, hydrologic, and ecologic modeling. *J. Appl. Meteor.,* **38,** 1474–1487.

——, and M. Sturm, 1998: A snow-transport model for complex terrain. *J. Glaciol.,* **44,** 498–516.

——, J. P. McFadden, M. Sturn, and R. A. Pielke, 2002: Modelled changes in arctic tundra snow, energy and moisture fluxes due to increased shrubs. *Global Change Biol.,* **8,** 17–32.

Luce, C. H., and D. G. Tarboton, 2004: An application of depletion curves for parameterization of subgrid variability of snow. *Hydrol. Processes,* **18,** 1409–1422.

Manabe, S., 1969: Climate and ocean circulation. Part I: The atmospheric circulation and the hydrology of the earth's surface. *Mon. Wea. Rev.,* **97,** 739–744.

Marks, D., T. Link, A. Winstral, and D. Garen, 2001: Simulating snowmelt processes during rain-on-snow over semi-arid mountain basin. *Ann. Glaciol.,* **32,** 195–202.

Marsh, P., and J. W. Pomeroy, 1996: Meltwater fluxes at an arctic forest-tundra site. *Hydrol. Processes,* **10,** 1383–1400.

McCartney, S. E., 2006: Spatial variability of snowmelt water balances in a subarctic catchment. M.S. thesis, University of Saskatchewan, Saskatoon, Saskatchewan, Canada, 125 pp.

——, S. K. Carey, and J. W. Pomeroy, 2006: Intra-basin variability of snowmelt water balance calculations in a subarctic catchment. *Hydrol. Processes,* **20,** 1001–1016.

Pietroniro, A., and Coauthors, 2007: Development of the MESH modelling system for hydrological ensemble forecasting of the Laurentian Great Lakes at the regional scale. *Hydrol. Earth Syst. Sci.,* **11,** 1279–1294.

Pohl, S., B. Davison, P. Marsh, and A. Pietroniro, 2005: Modelling spatially distributed snowmelt and meltwater runoff in a small arctic catchment with a hydrology–land surface scheme (WATCLASS). *Atmos.–Ocean,* **43,** 193–211.

Pomeroy, J. W., P. Marsh, and D. M. Gray, 1997: Application of a distributed blowing snow model to the Arctic. *Hydrol. Processes,* **11,** 1451–1464.

——, J. Parviainen, N. Hedstrom, and D. M. Gray, 1998: Coupled forest snow interception and sublimation. *Hydrol. Processes,* **12,** 2317–2337.

——, B. Toth, R. J. Granger, N. R. Hedstrom, and R. L. H. Essery, 2003: Variation in surface energetics during snowmelt in a subarctic mountain catchment. *J. Hydrometeor.,* **4,** 702–719.

——, and Coauthors, 2006: Shrub tundra snowmelt. *Hydrol. Processes,* **20,** 923–942.

——, D. M. Gray, T. Brown, N. R. Hedstrom, W. Quinton, R. J. Granger, and S. K. Carey, 2007: The cold regions hydrological model: A platform for basing process representation and model structure on physical evidence. *Hydrol. Processes,* **21,** 2650–2667.

Quinton, W. L., T. Shirazi, S. K. Carey, and J. W. Pomeroy, 2005: Soil water storage and active-layer development in a subalpine tundra hillslope, southern Yukon Territory, Canada. *Permafrost Periglacial Processes,* **16,** 369–382.

Sicart, J. E., J. W. Pomeroy, R. L. H. Essery, and D. Dewley, 2006: Incoming longwave radiation to melting snow: Observations,

sensitivity and estimation in northern environments. *Hydrol. Processes,* **20,** 3697–3708.

Sivapalan, M., and R. A. Woods, 1995: Evaluation of the effects of general circulation models' subgrid variability and patchiness of rainfall and soil moisture on land surface water balance fluxes. *Hydrol. Processes,* **9,** 697–717.

Slater, G., and Coauthors, 2001: The representation of snow in land surface schemes: Results from PILPS 2(d). *J. Hydrometeor.,* **2,** 7–25.

Soulis, E. D., K. R. Snelgrove, N. Kouwen, F. Seglenieks, and D. L. Verseghy, 2000: Towards closing the vertical water balance in Canadian atmospheric models: Coupling of the land surface scheme CLASS with the distributed hydrological model WATFLOOD. *Atmos.–Ocean,* **38,** 251–269.

Sturm, M., J. P. McFadden, G. E. Liston, F. S. Chapin, C. H. Racine, and J. Holmgren, 2001: Snow–shrub interactions in arctic tundra: A hypothesis with climate implications. *J. Climate,* **14,** 336–344.

Tolson, B. A., and C. A. Shoemaker, 2007: Dynamically Dimensioned Search algorithm for computationally efficient watershed model calibration. *Water Resour. Res.,* **43,** W01413, doi:10.1029/2005WR004723.

Verseghy, D. L., 1991: CLASS—A Canadian land surface scheme for GCMs. I. Soil model. *Int. J. Climatol.,* **11,** 111–133.

——, N. A. McFarlane, and M. Lazare, 1993: CLASS—A Canadian land surface scheme for GCMs. II. Vegetation model and coupled runs. *Int. J. Climatol.,* **13,** 347–370.

Wood, E. F., 1995: Scaling behaviour of hydrological fluxes and variables: Empirical studies using hydrological model and remote sensing data. *Hydrol. Processes,* **10,** 21–36.